GSA DATA REPOSITORY 2017051

Local glaciation in West Greenland linked to North Atlantic Ocean circulation during the Holocene

Avriel D. Schweinsberg[1], Jason P. Briner[1], Gifford H. Miller[2], Ole Bennike[3], and Elizabeth K. Thomas[1,4]

[1]*Department of Geology, University at Buffalo, Buffalo, NY 14260, USA*
[2]*Department of Geological Sciences, University of Colorado, Boulder, CO 80309, USA*
[3]*Geological Survey of Denmark and Greenland, Øster Voldgade 10, DK-1350 Copenhagen k, Denmark*
[4] *Department of Geosciences, University of Massachusetts, Amherst, MA 01003, USA*

1. Proglacial Lake Sediment Analysis

Sediment Core Collection and Analysis

Proglacial Sikuiui Lake (70.21ºN, 51.11º W, 604 m above sea level [asl]), eastern Nuussuaq, is fed primarily by an outlet glacier emanating from Qangattaq ice cap (Fig. 1, main text). Bedrock erosion by the Qangattaq glaciers provide the primary source of mineral-rich sediment to Sikuiui Lake, and increases in glacier size should clearly be reflected as increases in mineral-rich input. A 99.5 cm-long sediment core (13MCR-D3) was recovered from Sikuiui proglacial lake in August 2013 using a modified Universal Coring system (Fig. DR1; Nesje, 1992). Bathymetry data were collected with a dual beam depth transducer and Garmin GPSMAP 400 GPS device. The water depth at the coring site for 13MCR-D3 (Sikuiui Lake) was 9.62 meters.

Analyses of the sediments in Sikuiui Lake included measurements of physical, magnetic, and geochemical properties. Samples for loss-on-ignition (LOI) were extracted every 0.5 cm throughout each core. LOI is calculated as the difference between the mass of dried samples and their mass after heating for ~2.5 hours at 550 ºC (Smith, 2003), and is shown as the weight percent of sediment composed of organic material. Trends in LOI downcore are interpreted as changes in primary productivity loosely associated with summer temperature, as well as the dilution of organic matter by minerogenic sediment input.

High-resolution photographs, magnetic susceptibility (MS; SI x 10^{-15}) and gamma density (g/cc) were measured at 0.2 cm intervals using a GEOTEK Core Scanner and Core Splitter in the Quaternary Laboratory at the University of Massachusetts-Amherst. Scanning X-ray

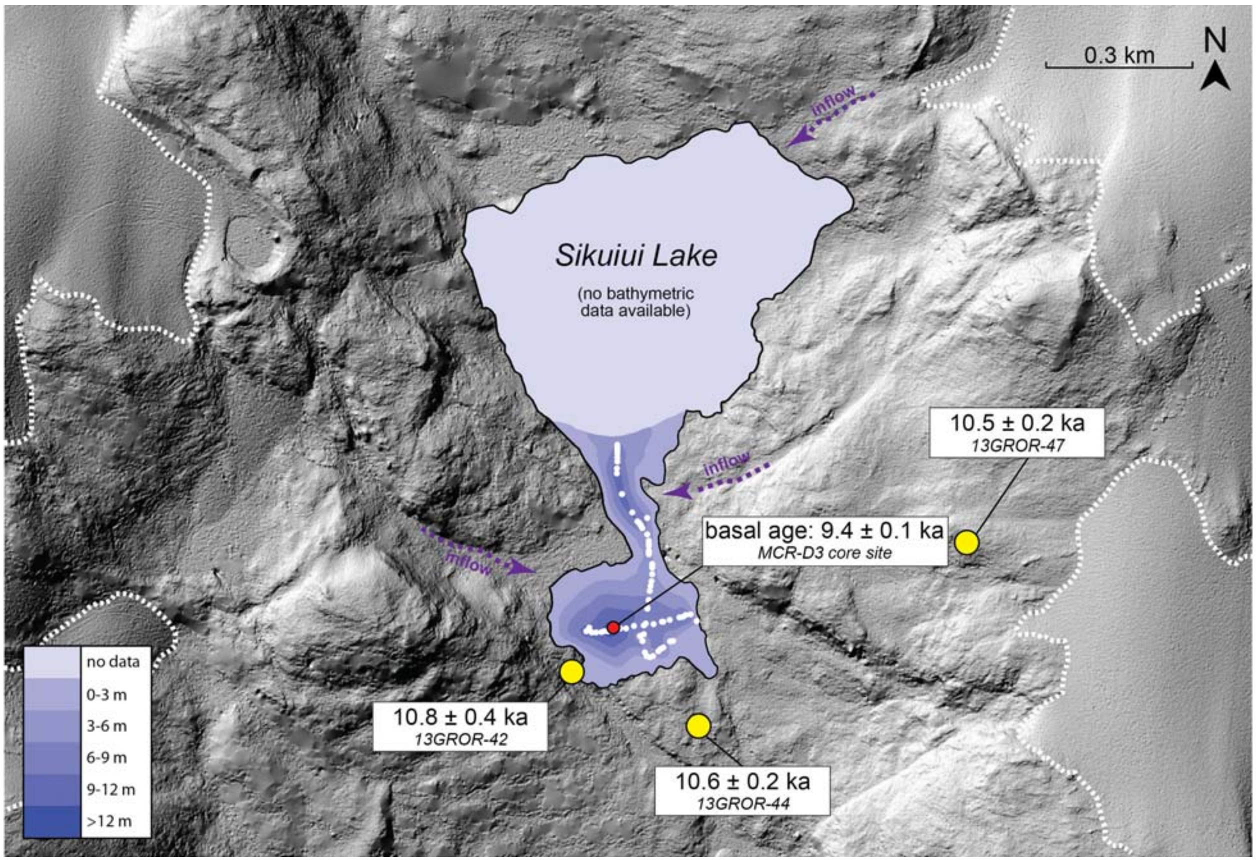

Figure DR1. Bathymetry map for Sikuiui Lake superimposed on a hillshade of a digital surface model (http://www.pgc.umn.edu/elevation/stereo/setsm; Noh et al., 2015). Bathymetric contours are three meters each and bathymetry measurement locations are illustrated by the white circles. Meltwater routes to Sikuiui Lake are shown by purple dashed lines. Red circle shows coring site and basal radiocarbon age for sediment core 13MCR-D3 (Table DR2). ^{10}Be ages on erratics resting on bedrock denoted by yellow circles (Table DR3). August 2014 local ice cap margins indicated by dashed white lines.

fluorescence (XRF) data was acquired using an Itrax nondestructive core scanner in the X-ray Fluorescence Laboratory at the University of Massachusetts-Amherst to produce profiles of relative elemental compositions (Croudace et al., 2006; Rothwell et al., 2006). A suite of 27 elements were measured: Al, Si, Ar, K, Ca, Ti, V, Cr, Mn, Fe, Ni, Cu, Zn, Ge, Rb, Sr, Y, Zr, Pd, Ba, La, Ce, Pr, Nd, Sm, Dy, Er. Our analysis focused only on Si, K, Ca, Ti, Mn, Fe, Zn, Rb, and Sr, which have detection limits that range from 150 to 5 ppm and robust peak integral count rates (Croudace et al., 2006). 13MCR-D3 was scanned at 0.2 cm intervals with voltage of 30 kV, current of 55 nA, and an exposure time of 10 seconds.

Chronology

Twelve radiocarbon ages of aquatic macrofossils were acquired from core 13MCR-D3 (Table DR2). Aquatic macrofossils were isolated from surrounding sediment using deionized water washes through sieves. Samples were then freeze-dried before transport to the National Ocean Sciences Accelerator Mass Spectrometry Facility (NOSAMS) at Woods Hole Oceanographic Institution. Aquatic macrofossils were used in order to avoid dating potentially old terrestrial material washed in from the surrounding landscape. A hard-water effect is possible in our field area but unlikely to be significant because the catchment is dominated by gneissic terrain, and the study area is well above the marine limit; therefore, it is unlikely that the radiocarbon ages were affected by old carbon sourced from bedrock, marine water or surrounding marine sediments.

The Sikuiui Lake age-depth model (Fig. DR2) was constructed by fitting the radiocarbon ages with a smooth spine function (smoothing level = 0.2) using the CLAM 2.2 code (Blaauw, 2010) in the statistical software package 'R.' The radiocarbon-dated samples were calibrated using the IntCal13 calibration curve with atmospheric data from Reimer et al. (2013), and are reported as the median of the 2σ range ± one half of the 2σ range.

Scanning XRF Data Analysis

We employed Principal Component Analysis (PCA; Fig DR3) to detect patterns of variability that are shared between the investigated lake sediment variables (i.e., Vasskog et al., 2012; Røthe et al., 2015). We included all times series that have an analytically robust signal in the PCA, excluding only the time series that have poor analytical measurements, or that have a low signal-to-noise ratio (Croudace et al., 2006). The variables that met these requirements included Si, K, Ca, Ti, Mn, Fe, Rb, and Sr, and physical sediment variables LOI and logMS (Fig. DR3), resulting in a final dataset containing 10 different variables with a stratigraphical resolution of 0.5 cm. LogMS was used due to a large range of values in the raw data (MS values from -1.58 to 442.15 (SI x 10^{-5})). A weak reaction to changing water content has been observed for K and Ti in previous lake sediment studies (Vasskog et al., 2012); however, this effect is negated if they are combined in a ratio (K/Ti), because of their similar atomic numbers and thus similar x-ray attenuation properties. Thus, we chose to include the K/Ti ratio in our analysis.

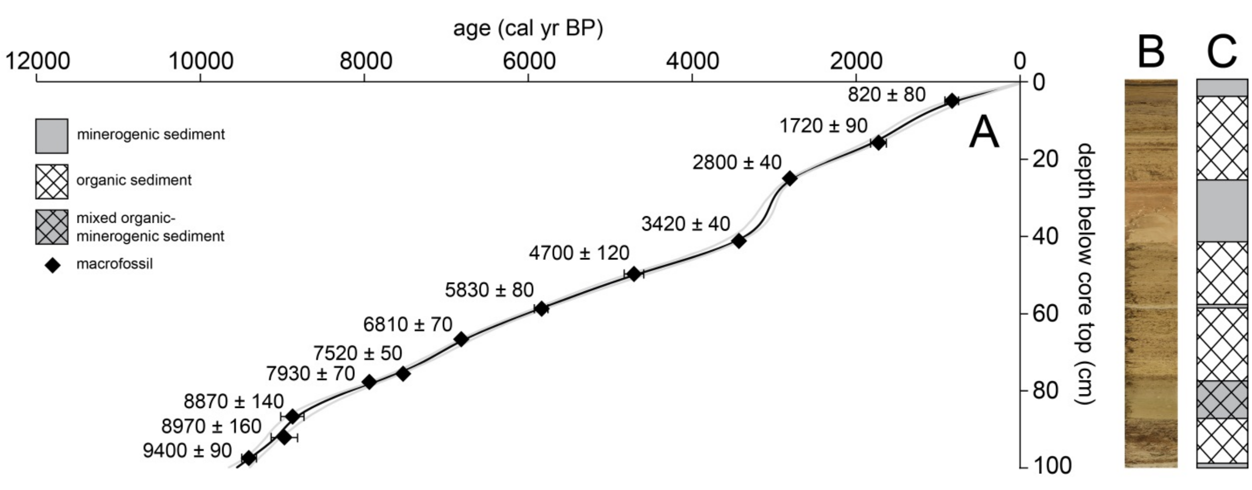

Figure DR2. **(A)** Age-depth model for Sikuiui Lake. Light gray lines depict 95% confidence intervals for CLAM 2.2 smooth spline function. Radiocarbon ages (cal yr BP; black diamonds) are reported as the median of the 2σ range ± one half of the 2σ range (Table DR2). **(B)** Sikuiui sediment core photograph. **(C)** Sediment core log for Sikuiui Lake interpreted from core stratigraphy.

Gamma density was not included in the PCA due to the data gaps present in the lake sediment record (Fig. DR4). Higher resolution datasets (MS, XRF elemental data) were downsampled to obtain the same resolution as the parameter with the lowest resolution (LOI) prior to PCA.

Figure DR3 shows the biplot of PCA results from Sikuiui Lake against the first and second Principal Component axes, which are the two dimensions most likely to reflect signals of interest. Table DR1 shows the factor loadings for the first five Principal Components. The first Principal Component (PC1) explains 56% of the total variability of the dataset for Sikuiui Lake, implying that the dataset contains a strong common signal that is reflected in many of the variables. In the biplot of the first and second Principal Components (PC1 and PC2; Fig. DR3), it can also be observed how the different parameters correlate with each other within these two dimensions, expressed as the angle between the variable vectors (90° = virtually no correlation, 0° or 180° = very high positive or negative correlation, respectively).

Correlations between the 10 variables in the PCA, as reflected in the strong signal captured by PC1, suggests that a single process is responsible for the bulk of the observed changes in the lake record (Fig. DR3; Table DR1). Variations along the first PCA axis (PC1) are considered to be the most robust reflection of the multi-proxy dataset obtained from Sikuiui Lake, and are interpreted to reflect variations in glacier extent in the upstream catchment through time (Fig. DR4). The trends in PC1 are similar to those in magnetic susceptibility and density, parameters typically used to reconstruct glacier size (e.g., Dahl et al., 2003), justifying the use of PC1 scores to infer past minerogenic changes (Fig. DR4). PC1 scores co-vary with fluctuations in silica, suggesting that the majority of silica in the lake record is sourced from local bedrock, and, consequently, that PC1 scores track glacier input (Fig. DR4). PC1 scores also co-vary with fluctuations in titanium, an element unaffected by within-lake production and therefore indicative of sediment transport to the lake, further supporting that PC1 scores track lithogenic input to Sikuiui Lake. Furthermore, high PC1 scores are correlated with mineral-rich sections of the core, and low PC1 values are associated with organic-rich sediments (Figs. DR2 and DR4). The fact that the PCA independently arrives at the conclusion supported by both physical parameters and visible changes in stratigraphy justifies our use of PC1 to infer past minerogenic changes and track changes in glacier size despite accounting for only 56% of variance.

PC2 explains about 23% of the variance for Sikuiui Lake, and likely reflects variability in redox conditions in the lake throughout the Holocene as Fe and Mn are redox sensitive elements. Although Mn, Fe and Rb are not correlated with minerogenic changes (Fig. DR3), we do not exclude them from the PCA given their high signal-to-noise ratios and peak integral count rates (Croudace et al., 2006).

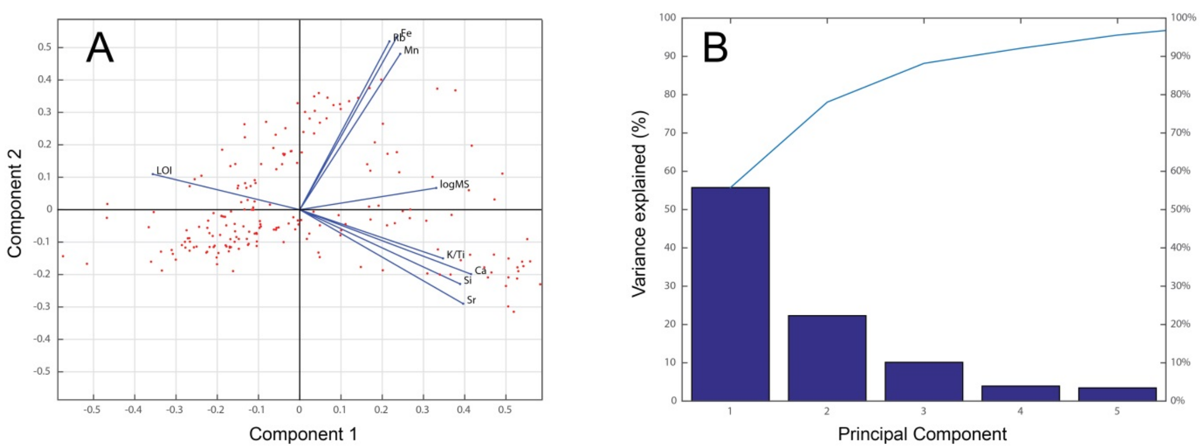

Figure DR3. (A) Sikuiui Lake biplot showing the results of the Principal Component Analysis (PCA) for the first and second Principal Component axes. Red dots represent samples. **(B)** Scree plot of PCA results from Sikuiui Lake.

Interpreting sedimentation in proglacial lakes

Proglacial lakes that receive meltwater from ice sheets and glaciers archive continuous records of sediment deposition that are frequently used to develop records of past environmental conditions and glacier activity during the Holocene (Nesje et al., 2000; Dahl et al., 2003; Bakke et al., 2005; Geirsdottir et al., 2013; Briner et al., 2010; Balascio et al., 2015). This work focuses on utilizing lake sediments as indices of glacier size, and relies on the assumption that large glaciers produce more minerogenic material and meltwater than small glaciers. The relative quantities of organic matter versus inorganic clastic material are interpreted to reflect the waxing and waning of ice; clastic sediment amount increases (and/or organic matter production decreases) during periods of glacier advance, and vice versa. Therefore, increasing and decreasing minerogenic sediment flux to the lake should reflect changes in the contribution of minerogenic material eroded from catchment bedrock and delivered to the lake (Balascio et al., 2015).

Table DR1. Factor loadings on 13MCR-D3 PC axes (PC1 through PC5) for physical and scanning XRF elemental data.

	PC1	**PC2**	**PC3**	**PC4**	**PC5**
variance explained (%)	56	23	10	5	4
LOI	-0.36	0.11	-0.37	0.68	0.19
logMS	0.33	0.07	0.56	0.44	-0.45
Si	0.39	-0.23	-0.31	-0.15	0.20
Ca	0.42	-0.20	0.01	0.02	0.23
Mn	0.24	0.48	0.26	0.29	0.53
Fe	0.24	0.53	-0.16	-0.25	0.23
Rb	0.22	0.52	-0.33	-0.12	-0.53
Sr	0.40	-0.29	0.05	0.06	0.12
K/Ti	0.35	-0.15	-0.50	0.39	-0.20

Although we focus on utilizing lake sediments as indices of glacier size, sediments in proglacial lakes can be the result of a complex set of physical processes such as sediment storage, erosion, and transport within glacial and proglacial systems (i.e., Dahl et al., 2003). Sedimentation processes in a proglacial lake can be impacted by differences in glacier size, erosive ability, and meltwater production, all of which impact the amount and character of minerogenic sediment in proglacial lakes (Balascio et al., 2015). Mass wasting processes and the delayed release of stored sediment along the transport pathway to the lake also effect sedimentation processes in proglacial lakes. We recognize that these factors can complicate the mechanistic link between minerogenic input and glacier size in Sikuiui Lake. The input of sediment from non-glacial processes is restricted due to the proximity of the outlet glaciers to the lake and relatively small catchment (Fig. DR1), which limits the potential for sediment storage between the glaciers and Sikuiui Lake. The landscape surrounding Sikuiui Lake does have steep slopes, however the lack of age reversals and outliers in the age-depth model (Fig. DR2), and absence of turbidites and rapid changes in sediment accumulation, suggest that sedimentation to Sikuiui Lake was minimally affected by mass wasting events during the Holocene. Nevertheless, we cannot be sure that all mineral-rich sediment layers indicate glacier advance.

We assume that the outlet glaciers feeding Sikuiui Lake throughout the Holocene were primarily warm-based given the continuous deposition of sediment throughout our record, and geomorphological evidence (bedrock erosion, moraines) suggesting the presence of warm-based ice. However, the absence of evidence for glacial erosion and subglacial drainage (Ives, 1962), and the preservation of undisturbed pattern ground and rooted moss and vegetation (Falconer, 1966) found along high-elevation margins of the Qangattaq ice cap and other nearby ice caps indicates the presence of cold-based ice in certain sectors of ice caps throughout the study region. Ice cap margins located on high, relatively flat terrain between outlet glaciers in this region typically host cold-based ice and exhibit geomorphological characteristics typical of cold-based regimes (Ives, 1962; Falconer, 1966). Because the ice caps in this study host both lower elevation warm-based outlet glaciers and adjacent higher elevation cold-based margins, we acknowledge the possibility that glaciers feeding Sikuiui Lake may have experienced fluctuations in thermal regime through the Holocene, and in turn may have influenced the sedimentation in Sikuiui Lake. Similarly, the sedimentation to Sikuiui Lake may have been influenced by contributions from different ice cap lobes through time due to multiple meltwater routes to the lake (Fig. DR1). Despite the presence of varying thermal regimes in this region, we believe the record from Sikuiui Lake is robust given its close correlation with other proxies used in this study and continuous signal throughout the Holocene. For example, where elevated PC1 scores coincide with modes in moss radiocarbon ages, we can have high confidence that the mineral input to the Sikuiui Lake represents glacier advances. On the other hand, prior to ~5 ka, we have less confidence that mineral-rich layers represent glacier advances.

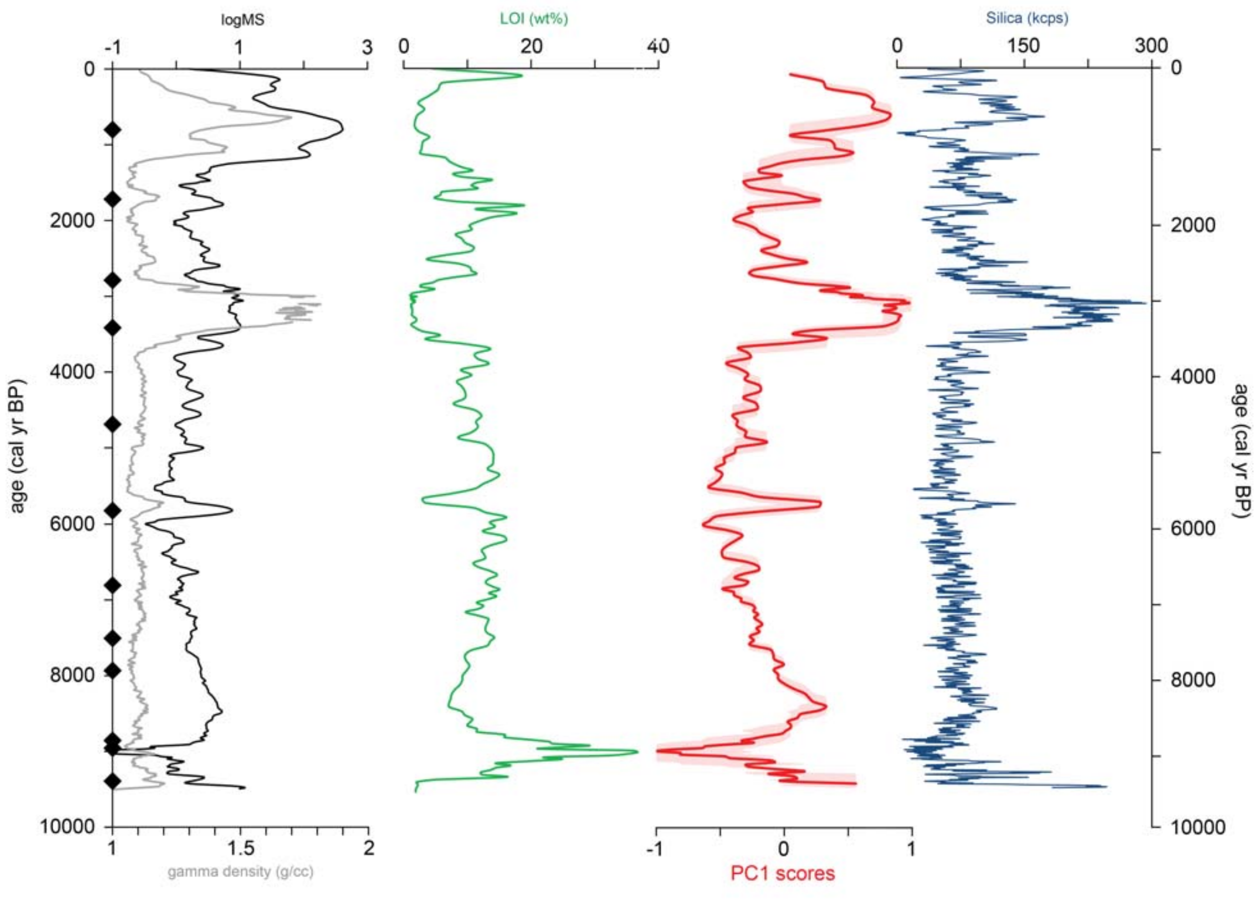

Figure DR4. Downcore data plotted vs. age for Sikuiui Lake. Physical parameters include magnetic susceptibility (plotted on a log scale; black curve), gamma density (gray curve), and LOI (green curve). Silica XRF elemental data (blue curve) is included in the PC1 scores (red curve; shading = 95% age uncertainty), along with nine other parameters. The locations of radiocarbon ages (black diamonds) are also shown.

Yellow panels in Figure 2 (main text) indicate all intervals in the sediment record that we interpret as glacier advances. Our interpretations for these intervals are based on three factors: PC1 scores greater than zero, correlation with the in-situ moss record and ^{10}Be ages, and the visual stratigraphy in the sediment core. An advantage of our study is our ability to identify glacier advances from three independent proxies, and therefore we are most confident in the timing of glacier advances throughout the past 5 ka. By bringing together all three methods, we highlighted intervals in the Sikuiui Lake record that a) exhibit elevated PC1 scores, b) occur in-step with or just following peaks in the in-situ moss record, c) are synchronous with ^{10}Be ages from the late Holocene moraines (where available), and d) are glacially-derived minerogenic sections of the core. We highlight specific intervals in the main text (~3.7, ~2.9, ~1.4 ka and the LIA) because these are intervals that meet all of the requirements mentioned above, thus, we are the most confident in interpreting these as glacier advances. In contrast, we have added question marks to Figure 2 (main text) associated with peaks in PC1 scores at ~5.8 ka and during the interval between ~8.8-8.0 ka because these intervals occur prior to the oldest radiocarbon age in the in-situ moss chronology, and there is a lack of ^{10}Be-dated moraines coincident with these intervals.

2. Cosmogenic ^{10}Be exposure dating

Sample collection and geomorphic setting

Quartz-rich samples were collected using a hand sledge and chisel from the tops of tall and stable flat-topped moraine boulders (Uigorliup Lake valley) and erratics (resting on primary bedrock surfaces) in August 2013 (Fig. DR5). Erratics were sampled from moraine crests or high, windswept topographic locations in order to reduce uncertainty associated with snow or soil shielding. We avoided sampling from boulder edges and corners to limit the collection of any surfaces that may have experienced accelerated erosion. Erosion and spalling of sampled boulder surfaces is considered absent or minimal, as indicated by negligible surface pitting and the presence of glacial smoothing on most boulder surfaces. Geographic coordinates and sample elevations of each boulder were obtained using a handheld GPS with ±10 m vertical accuracy. A clinometer was used to measure shielding by surrounding topography and used to derive corrections for each sample site, which range from 0.988 to 0.992 (Uigorliup moraine boulders) and 0.994 to 0.995 (erratics). For details regarding geomorphic setting and assumptions for the Uigoriup Lake valley moraine complex, refer to the main text and supplementary file from Young et al. (2015).

^{10}Be ages of erratics outboard of Sikuiui Lake yield identical ages, within uncertainties, of ~10.6±0.2 ka (*n*=3; Fig. DR1; Table DR3), and ^{10}Be ages of two erratics outboard of the Uigorliup moraines agree within uncertainty and average 10.2±0.2 ka (*n*=2; Table DR3).

Geochemistry and ^{10}Be age calculations

All physical and chemical preparation of ^{10}Be samples was conducted at the University at Buffalo Cosmogenic Isotope Laboratory following well-established protocols. Average sample thickness was measured for each sample collected. Samples were crushed and then sieved to 250-800 μm. Quartz was isolated following procedures modified from Kohl and Nishiizumi (1992). Crushed samples were pretreated in dilute HCl and HF/HNO_3 prior to quartz isolation by heavy-liquid mineral separation and repeat etching in a 2% HF/1% HNO_3 solution.

Prior to the beryllium extraction steps, the etched quartz was tested for purity by ICP-AES at the LEGS facility at the University of Colorado-Boulder. Once verified as clean, 9Be carrier (~0.6 g; GFZ, 372.5 ± 3.5 ppm) was added to the purified quartz samples before dissolution in concentrated HF. Beryllium was extracted from samples using ion-exchange chromatography, selective precipitation, and oxidation to BeO.

All AMS measurements of $^{10}Be/^{9}Be$ (normalized to standard 07KNSTD3110; Nishiizumi et al., 2007) were obtained at the Lawrence Livermore National Laboratory Center for Accelerator Mass Spectrometry (LLNL-CAMS). Uigorliup moraine samples 13GROR-48, 49, 50, 55 and 56 (n=5) were run with a process blank that yielded a $^{10}Be/^{9}Be$ ratio of 1.9×10^{-15}.

Table DR2. Radiocarbon ages from Sikuiui Lake.

Core	Depth (cm)	Lab Number	Material Dated	Fraction Modern	$\delta^{13}C$ (‰ PDB)	Radiocarbon Age (14C yr BP)	Calibrated Age (cal yr BP ± 2σ)	Calibrated Age Ranges (cal yr BP ± 2σ)
13MCR-D3	14.0 - 14.5	OS-106899	Plant macrofossils	0.8949	-25.67	890 ± 20	820 ± 80	737 - 803, 810 - 830, 858 - 904
13MCR-D3	25.0 - 25.5	OS-106900	Plant macrofossils	0.7993	-22.32	1800 ± 20	1720 ± 90	1631 - 1652, 1694 - 1816
13MCR-D3	34.25-34.75	OS-110852	Plant macrofossils	0.7149	-24.04	2690 ± 20	2800 ± 40	2756 - 2809, 2814 - 2844
13MCR-D3	50.5 - 51.0	OS-106901	Plant macrofossils	0.6712	-21.53	3200 ± 25	3420 ± 40	3373 - 3458
13MCR-D3	59.0 - 59.5	OS-117858	Plant macrofossils	0.5963	-21.82	4150 ± 20	4700 ± 120	4585 - 4598, 4610 - 4768, 4782 - 4821
13MCR-D3	68.0 - 68.5	OS-106872	Plant macrofossils	0.5312	-21.23	5080 ± 30	5830 ± 80	5747 - 5833, 5841 - 5907
13MCR-D3	76.0 - 76.5	OS-116885	Plant macrofossils	0.4758	-22.84	5970 ± 25	6810 ± 70	6741 - 6864, 6866 - 6881
13MCR-D3	85.0 - 85.5	OS-110853	Plant macrofossils	0.4374	-23.10	6640 ± 30	7520 ± 50	7470 - 7575
13MCR-D3	87.25 - 87.75	OS-116884	Plant macrofossils	0.4128	-21.89	7110 ± 30	7930 ± 70	7866 - 7899, 7923 - 7999
13MCR-D3	96.0 - 96.5	OS-106873	Plant macrofossils	0.3684	-25.22	8020 ± 40	8870 ± 140	8729 - 8733, 8754 - 9016
13MCR-D3	101.5 - 102.0	OS-116949	Plant macrofossils	0.3655	-26.17	8090 ± 35	8970 ± 160	8810 - 8824, 8874 - 8876, 8978 - 9127
13MCR-D3	107.0 - 107.5	OS-106902	Plant macrofossils	0.3518	-27.40	8390 ± 40	9400 ± 90	9304 - 9364, 9367 - 9489

The remaining Uigorliup samples (n=4; 13GROR-51, 52, 54, and 54) were run with two process blanks that yielded an average $^{10}Be/^{9}Be$ ratio of 1.4×10^{-15} (average of 1.9×10^{-15} and 1.0×10^{-15}). ^{10}Be samples from erratics (13GROR-42, 44, 47, 80, 81) were run with a process blank that yielded a $^{10}Be/^{9}Be$ ratio of 2.7×10^{-15}. AMS uncertainty for blank-corrected Uigorliup moraine sample $^{10}Be/^{9}Be$ ratios range from 3.6-13.1% whereas AMS uncertainty ranges between 1.7-3.5% for erratics.

The ^{10}Be ages were derived using the CRONUS-Earth online ^{10}Be exposure age calculator (Balco et al., 2008; http://hess.ess.washington.edu/; Version 2.2; Table DR2). ^{10}Be ages were calculated using the locally-derived Baffin Bay production rate (Young et al., 2013; 3.96 ± 0.07 atoms g^{-1} a^{-1}) and time-variant 'Lm' scaling (Niishiizumi et al., 1989; Lal, 1991; Stone, 2000). Table DR3 details ^{10}Be ages calculated with alternative scaling schemes.

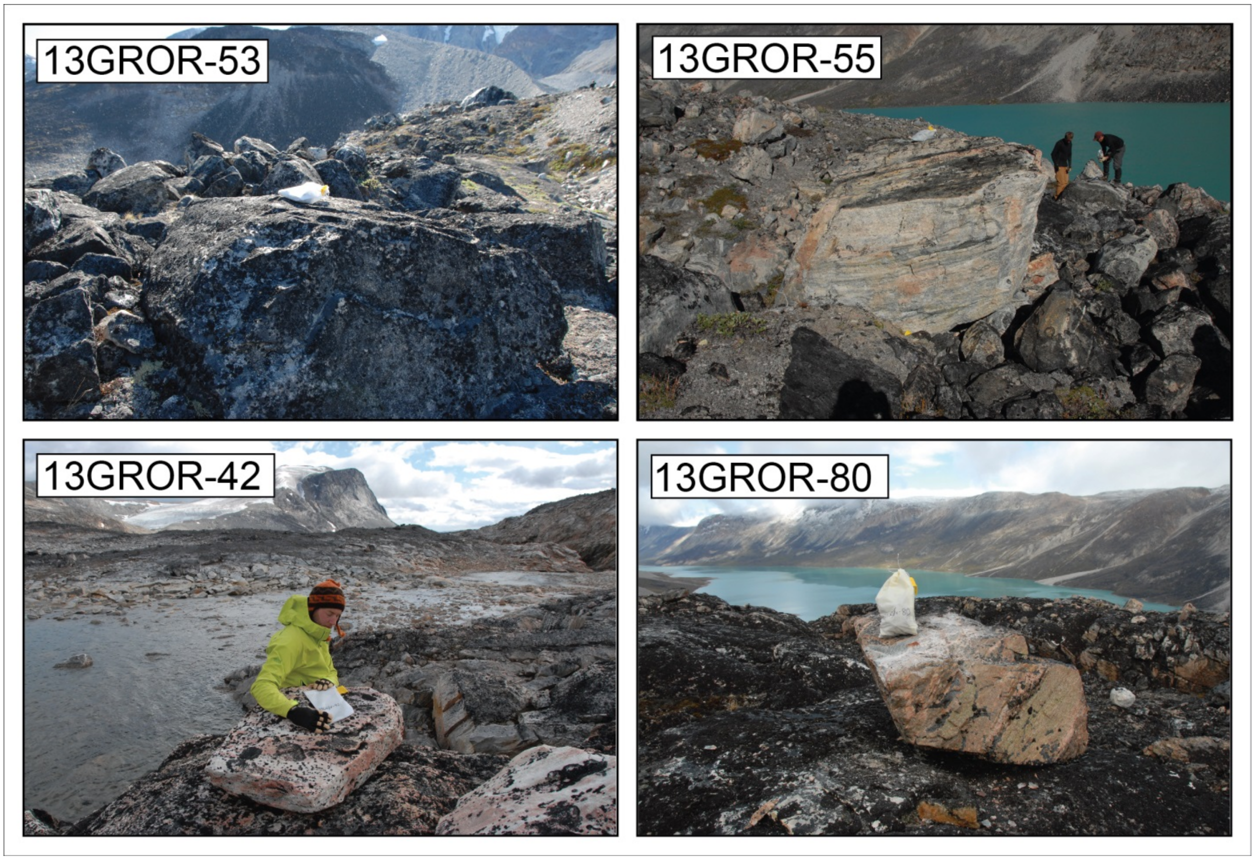

Figure DR5. Photographs of selected moraine boulders and erratics sampled for ^{10}Be-dating in this study. *13GROR-53 and 13GROR-55*: Samples from moraine crests in Uigorliup Lake valley (Young et al., 2015). *13GROR-42*: Erratic perched on bedrock southeast of Sikuiui Lake (Fig. DR1). *13GROR-80*: Sampled erratic perched on bedrock outboard of the Uigorliup moraines.

Table DR3. Beryllium-10 sample information and ages.

Sample ID	Latitude (deg. N)	Longitude (deg. W)	Elevation (m.a.s.l.)	Quartz (g)	Thickness (cm)	Shielding correction	Carrier added[a]	[Be-10] (atoms g^{-1})	+/- (atoms g^{-1})	Age (Lm) (yr/BP)[b]	+/- (yr/BP)
Nuussuaq deglaciation (Sikuiui Lake)											
59-13GROR-42	70.21106	-51.12485	612.0	23.7038	1.5	0.995	0.6242	8.43E+04	2.99E+03	10840	390
59-13GROR-44	70.21031	-51.11792	629.0	21.5749	2.0	0.993	0.6152	8.30E+04	1.42E+03	10560	180
59-13GROR-47	70.21385	-51.09491	799.9	14.7009	1.5	0.995	0.6126	9.72E+04	1.67E+03	10520	180
Bedrock knoll outboard Uigorliup moraines											
59-13GROR-80	70.24507	-51.22259	524.8	16.1214	1.0	0.994	0.6169	7.26E+04	1.88E+03	10100	260
59-13GROR-81	70.24532	-51.22328	505.0	23.9151	2.0	0.994	0.6135	7.27E+04	1.43E+03	10390	210
Uigorliup moraines - distal											
54-13GRO-48	70.25044	-51.22274	321.2	28.5944	2.0	0.992	0.6080	7.48E+03	4.46E+02	1280	80
54-13GRO-49	70.25035	-51.22226	317.1	18.1053	1.5	0.992	0.6087	5.31E+03	5.62E+02	910	100
54-13GRO-50	70.25103	-51.22182	313.5	29.6874	1.0	0.992	0.6055	6.53E+03	4.52E+02	1120	80
Uigorliup moraines – intermediate											
61-13GRO-51	70.25050	-51.22327	321.4	40.3426	2.0	0.992	0.6061	5.37E+03	3.93E+02	920	70
61-13GRO-52	70.25045	-51.22325	321.9	73.1059	1.8	0.992	0.6088	8.20E+03	2.94E+02	1400	50
61-13GRO-53	70.25042	-51.22329	322.4	37.8101	1.0	0.992	0.6085	7.99E+03	4.24E+02	1350	70
Uigorliup moraines – proximal											
61-13GRO-54	70.25004	-51.22425	329.1	69.1898	1.0	0.992	0.6080	4.99E+03	2.42E+02	840	40
54-13GRO-55	70.25116	-51.22250	316.9	16.4396	2.0	0.988	0.6065	5.18E+03	6.05E+02	890	100
54-13GRO-56	70.25120	-51.22227	316.2	13.9019	2.0	0.988	0.6076	5.24E+03	6.84E+02	900	120

[a] Samples were prepared using a carrier with a ^{9}Be concentration of 372.5 ppm.

[b] ^{10}Be ages are calculated using the Baffin Bay production rate and 'Lm' scaling (3.96 ±0.07 g^{-1} yr^{-1}; Young et al. 2013), standard air pressure 'std,' a sample density of 2.65 g cm^{-3}, and an effective attenuation length of 160 g cm^{-2}. We assume zero erosion over these timescales. All ^{10}Be concentrations are reported relative to 07KNSTD with a reported ratio of 2.85 x 10^{-12} using a ^{10}Be half-life of 1.36 x 10^{6} years (Nishiizumi et al., 2007). ^{10}Be ages from the Uigorliup moraines were originally reported by Young et al. (2015).

Table DR4. Comparison of ^{10}Be exposure ages (yrs) calculated under alternative scaling schemes. See Balco et al. (2008) for documentation of all five scaling schemes.

Sample ID	Lm (Table DR2)	De	Du	Li	St
Nuussuaq deglaciation (Sikuiui Lake)					
59-13GROR-42	10840 ± 390	10980 ± 390	10960 ± 390	10960 ± 390	10840 ± 390
59-13GROR-44	10560 ± 180	10700 ± 180	10680 ± 180	10670 ± 180	10560 ± 180
59-13GROR-47	10520 ± 180	10660 ± 180	10630 ± 180	10600 ± 180	10520 ± 180
Bedrock knoll outboard Uigorliup moraines					
59-13GROR-80	10100 ± 260	10220 ± 260	10200 ± 260	10200 ± 260	10100 ± 260
59-13GROR-81	10390 ± 210	10510 ± 210	10590 ± 210	10500 ± 210	10390 ± 210
Uigorliup moraines - distal					
54-13GRO-48	1280 ± 80	1290 ± 80	1290 ± 80	1260 ± 80	1280 ± 80
54-13GRO-49	910 ± 100	910 ± 100	910 ± 100	890 ± 100	910 ± 100
54-13GRO-50	1120 ± 80	1120 ± 80	1120 ± 80	1100 ± 80	1120 ± 80
Uigorliup moraines - intermediate					
61-13GRO-51	920 ± 70	920 ± 70	920 ± 70	900 ± 70	920 ± 70
61-13GRO-52	1400 ± 50	1410 ± 50	1410 ± 50	1380 ± 50	1400 ± 50
61-13GRO-53	1350 ± 70	1360 ± 70	1360 ± 70	1330 ± 70	1350 ± 70
Uigorliup moraines - proximal					
61-13GRO-54	840 ± 40	840 ± 40	840 ± 40	830 ± 40	840 ± 40
54-13GRO-55	890 ± 100	900 ± 100	900 ± 100	880 ± 100	890 ± 100
54-13GRO-56	900 ± 120	910 ± 120	910 ± 120	890 ± 120	900 ± 120

3. West Greenland moss chronology

Sample collection and methodology

A key method utilized in this study is radiocarbon dating of rooted tundra moss that has been recently exposed by receding ice cap margins in order to constrain spatio-temporal patterns of persistent cold-summer perturbations in western Greenland. In August 2013 we made 110 collections of *in situ* mosses following field protocols outlined in Miller et al. (2013a, b) from 34 separate ice caps, ranging from 760 to 1500 meters above sea level. Of these collections we obtained 54 radiocarbon ages, which are reported here, from 22 ice caps, ranging from 760 to 1500 meters above sea level (Figs. DR6 and DR7; Table DR4). We selected ice caps at different elevations and of different sizes to examine the regional extent of ice expansion in response to climate change during the late Holocene. Samples were collected along margins of small cold-based ice caps, or sectors of polythermal ice caps, that mantle relatively flat terrain in the Uummannaq Fjord region, the Nuussuaq peninsula, and Disko island (Fig. DR6). Small ice caps serve as ideal candidates for sampling because they are typically frozen to their beds, exhibit little or no ice flow, and consequently preserve relict landscapes with rooted tundra moss that was alive at the time of ice-cap expansion (see these references for more discussion on sampling protocols and interpretations: Anderson et al., 2008; Miller et al., 2013a, b). Changes in glacier dimensions in this region are likely a direct response to summer melt (Koerner, 205) due to the relatively small contribution of short-wave radiation and the associated melt-albedo feedback to summer melting (van de Berg et al., 2011). Therefore, we interpret changes in glacier size and snowline elevation as a proxy for summer temperature change in West Greenland.

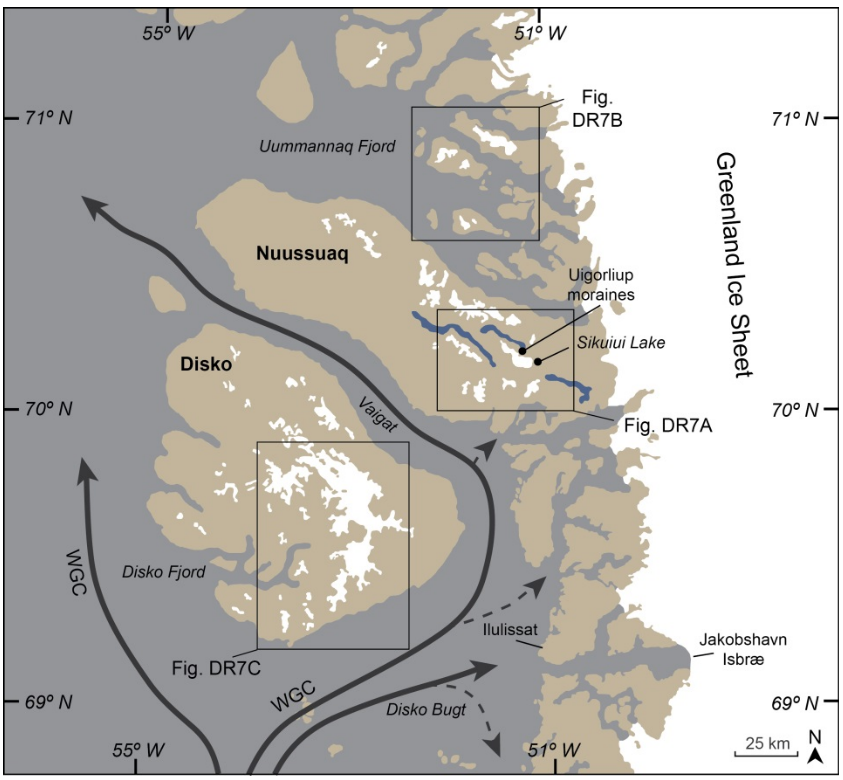

Figure DR6. Central West Greenland; West Greenland Current (WGC) depicted after Perner et al. (2013). Black boxes indicate areas shown in detail in Figure DR7.

We targeted *Polytrichum hyperboreum* for sampling due to its relatively brief life cycle (Miller et al., 2013a), however other moss genus were sampled and dated in the absence of

Polytrichum (Table DR4). We avoided sampling woody plants because their survival potential is much greater than for moss, and their woody stems carry an average radiocarbon age older than their kill date (LaFarge et al., 2013). For example, radiocarbon ages on three adjacent rooted plants recently emerging beneath a glacier in the Canadian Arctic include two moss taxa for which the ages are concordant, and an age on *Salix arctica*, that is 200 years older (LaFarge et al., 2013). This suggests that radiocarbon ages on woody plants reflect the average duration of the plants life, which can be decades to centuries, whereas mosses that die naturally are rapidly lost from the landscape (via water or wind) in most settings (Miller et al., 2013b). Dating a single moss stem is often more reliable because the radiocarbon age generally reflects a single year. Samples were typically collected within one meter of the present ice margin to ensure the mosses were exposed during the year of collection and avoid altered radiocarbon activity by regrowth (Miller et al., 2013a).

In the lab, isolation of macrofossils followed standard procedures of wet sieving in deionized water to remove sediment and gentle sonication when necessary. Where possible, a single stem of moss was of sufficient mass and selected for dating to minimize the change of dating a mixed-age sample. All 54 samples were then treated with an acid-base-acid wash, combusted, and converted to graphite at the National Ocean Sciences Accelerator Mass Spectrometry Facility (NOSAMS) at Woods Hole Oceanographic Institution. Radiocarbon ages were calibrated using the downloadable version of CALIB 7.0 with the IntCal13 calibration curve (Reimer et al., 2013). All calibrated ages are reported as the median age $\pm 1\sigma$ uncertainty (Table DR4) and expressed as a summed probability density function (PDF) generated by CALIB 7.0.

Successively younger radiocarbon age clusters in the West Greenland moss chronology (Fig. 2, main text) require subsequent summers to have been cooler than those prior to ice expansion on a multidecadal average (Miller et al., 2013b). This allows the derivation of the relative change in snowline, which is approximately coincident with the equilibrium-line altitude

(ELA) for mountain ice caps (dashed line, Fig. 2, main text; Miller et al., *in press*). The dashed line is a conceptual view of the relative change in ELA over the past 5 ka, which was constructed by following several rules: (1) a step down in snowline is centered on a cluster of radiocarbon ages, (2) the duration of the cold interval is set to be equal to the duration of each radiocarbon age cluster, and (3) snowline rise occurs in the gaps between radiocarbon age clusters, with the rise in magnitude being shorter than the previous step down such that overall there is net snowline lowering through the record. The ELA, or relative change in snowline, is schematic, not scaled, and only a qualitative interpretation.

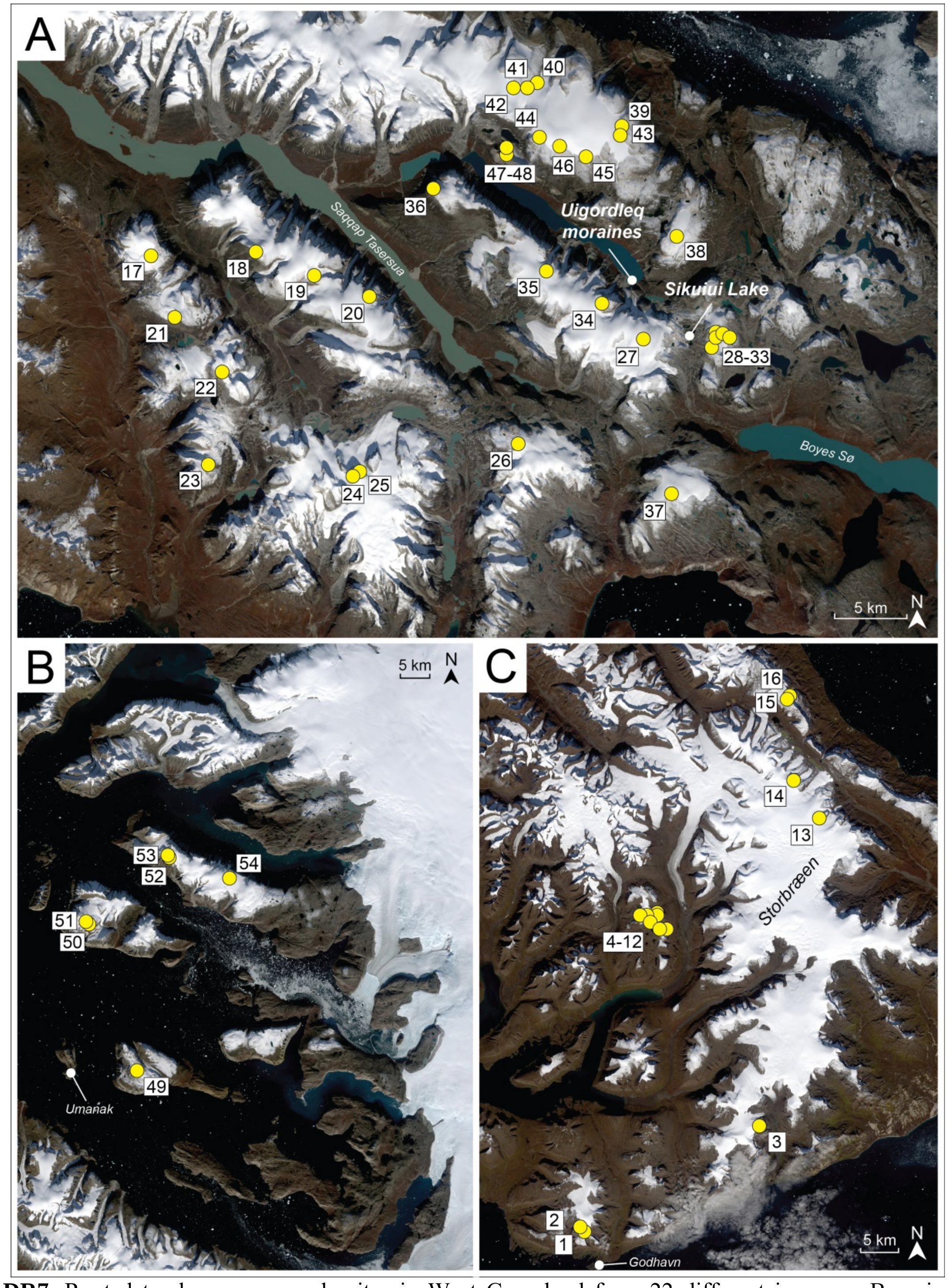

Figure DR7. Rooted tundra moss sample sites in West Greenland from 22 different ice caps. Base image is a LANDSAT8 natural color composite (RGB; 432) acquired on 09/03/2015. **(A)** Sample sites from eastern Nuussuaq (*n*=32). **(B)** Sample locations in the Uummannaq Fjord region of West Greenland (*n*=6). **(C)** Sample sites on the Disko island (*n*=16). Numbers refer to sample numbers on Table DR5.

Table DR5. Tabulation of 54 radiocarbon dates on rooted moss recently emerged from beneath glacier ice in West Greenland and their metadata. Sample numbers refer to Fig. DR7. Calibrated ages from Calib 7.0 with ± ranges representing 1σ uncertainties.

Sample #	Sample ID	Latitude (deg. N)	Longitude (deg. W)	Elev. (m asl)	Location	Material Dated	Distance from ice edge (cm)	Lab ID	Fraction Modern	$\delta^{13}C$	^{14}C Age	Calibrated Age	Calibrated Age Ranges
1	10Lyng-1	69.28833	-53.59625	795.4	Disko Island	tundra moss	500	UCIAMS-84690	-	-	3405 ± 25	3650 ± 40	3614 - 3625, 3628 - 3650, 3658 - 3691
2	10Lyng-2	69.29000	-53.60040	823.5	Disko Island	*Polytrichum hyperboreum*	200	UCIAMS-84699	-	-	3280 ± 25	3520 ± 40	3475 - 3513, 3526 - 3558
3	13GRØv-02	69.42538	-52.99410	950.9	Disko Island	*Polytrichum hyperboreum*	400	OS-106358	0.6514	-25.03	3440 ± 25	3720 ± 80	3641 - 3672, 3677 - 3720, 3804 - 3806
4	13GRØv-08	69.67813	-53.41667	972.7	Disko Island	*Polytrichum hyperboreum*	20	OS-106271	0.9214	-23.21	660 ± 15	620 ± 50	569 - 582, 649 - 662
5	13GRØv-12	69.67996	-53.43274	1052.5	Disko Island	*Ditrichum flexicaule*	90	OS-109288	0.8275	-23.75	1520 ± 25	1420 ± 60	1356 - 1414, 1466 - 1475
6	13GRØv-14	69.68389	-53.38237	843.7	Disko Island	*Polytrichum hyperboreum, Pohlia cruda*	80	OS-106269	0.7822	-24.33	1970 ± 20	1920 ± 30	1890 - 1934, 1939 - 1941
7	13GRØv-18	69.67835	-53.38693	901.3	Disko Island	*Polytrichastrum alpinum*	80	OS-109289	0.9841	-24.14	130 ± 45	140 ± 130	13 - 40, 61 - 119, 122 - 147, 188 - 196, 212 - 233, 241 - 269
8	13GRØv-20	69.66468	-53.36767	1004.5	Disko Island	*Pogonatum dentatum*	200	OS-109290	0.6601	-26.73	3340 ± 25	3600 ± 40	3560 - 3615, 3623 - 3631
9	13GRØv-23	69.66446	-53.35700	1068.6	Disko Island	*Polytrichum hyperboreum*	20	OS-106359	0.7053	-25.15	2800 ± 25	2900 ± 40	2865 - 2929, 2938 - 2941
10	13GRØv-25	69.67398	-53.39941	867.9	Disko Island	*Polytrichum piliferum*	40000	OS-109291	0.9700	-24.94	245 ± 20	230 ± 70	160 - 161, 286 - 305
11	13GRØv-26	69.67398	-53.39943	868.7	Disko Island	*Salix arctica*	40000	OS-109292	0.9713	-26.78	235 ± 25	230 ± 70	155 - 166, 284 - 302
12	13GRØv-27	69.67413	-53.40079	875.3	Disko Island	*Pohlia cruda*	250	OS-106360	0.9583	-22.02	340 ± 25	420 ± 80	319 - 338, 348 - 392, 426 - 258
13	13GRØv-31	69.80752	-52.81346	1294.1	Disko Island	*Racomitrium lanuginosum*	250	OS-109293	0.7317	-22.88	2510 ± 25	2610 ± 110	2507 - 2529, 2536 - 2590, 2615 - 2634, 269 - 2720
14	13GRØv-35	69.85199	-52.91593	1412.8	Disko Island	*Racomitrium lanuginosum*	20	OS-106361	0.8010	-23.74	1780 ± 25	1680 ± 50	1626 - 1669, 1691 - 1727
15	13GRØv-36	69.95591	-52.93549	1432.5	Disko Island	*Polytrichum hyperboreum. Pohlia cruda*	20	OS-106272	0.6327	-26.37	3680 ± 35	3990 ± 20	3973 - 4014, 4018 - 4084

16	13GRØv-37	69.95321	-52.94776	1423.6	Disko Island	*Polytrichum hyperboreum*	150	OS-109336	0.6442	-24.65	3530 ± 35	3800 ± 70	3725 - 3752, 3760 - 3794, 3820 - 3868
17	13GRØv-38	70.26311	-52.10853	1100.3	Nuussuaq	*Pohlia cruda*	400	OS-106442	0.6562	-25.21	3380 ± 35	3630 ± 50	3579 - 3643, 3667 - 3682
18	13GRØv-42	70.26632	-51.91516	1351.1	Nuussuaq	*Polytrichum hyperboreum*	0	OS-109312	0.6670	-26.17	3250 ± 30	3480 ± 70	3410 - 3423, 3445 - 3494, 3503 - 3507, 3532 - 3555
19	13GRØv-43	70.25265	-51.81057	1242.2	Nuussuaq	*Polytrichum hyperboreum*	140	OS-106362	0.6459	-25.96	3510 ± 30	3780 ± 60	3723 - 3797, 3816 - 3836
20	13GRØv-44	70.24000	-51.70829	1188.9	Nuussuaq	*Polytrichum piliferum*	0	OS-109313	0.7004	-24.43	2860 ± 25	2970 ± 50	2926 - 3006, 3014 - 3023
21	13GRØv-47	70.22529	-52.06295	1248.3	Nuussuaq	*Polytrichum piliferum*	0	OS-106363	0.6542	-25.92	3410 ± 25	3660 ± 30	3632 - 3693
22	13GRØv-49	70.19211	-51.97383	1363.0	Nuussuaq	*Polytrichum piliferum*	2	OS-109365	0.6533	-25.25	3420 ± 30	3660 ± 40	3616 - 3621, 3631 - 3702
23	13GRØv-51	70.13477	-51.99700	1103.0	Nuussuaq	*Polytrichum hyperboreum*	0	OS-106364	0.6846	-25.92	3040 ± 30	3260 ± 70	3182 - 3195, 3207 - 3255, 3291 - 3330
24	13GRØv-52	70.13031	-51.72941	1277.3	Nuussuaq	*Polytrichum hyperboreum*	30	OS-109314	0.5994	-26.29	4110 ± 50	4670 ± 140	4529 - 4647, 4673 - 4697, 4760 - 4805
25	13GRØv-53	70.13076	-51.72757	1269.8	Nuussuaq	*Pogonatum urnigerum*	0	OS-106365	0.5955	-25.31	4160 ± 30	4720 ± 100	4628 - 4637, 4642 - 4682, 4687 - 4730, 4732 - 4744, 4746 - 4762, 4798 - 4821
26	13GRØv-54	70.15017	-51.43520	886.2	Nuussuaq	*Polytrichum hyperboreum*	0	OS-106366	0.8940	-25.08	900 ± 30	840 ± 70	767 - 802, 811 - 829, 860 - 904
27	13GRØv-56	70.21493	-51.20802	1120.7	Nuussuaq	*Polytrichum hyperboreum*	40	OS-106367	0.7358	-26.21	2460 ± 25	2580 ± 120	2459 - 2520, 2525 - 2539, 2587 - 2617, 2632 - 2699
28	13GRØv-58	70.20984	-51.08499	843.0	Nuussuaq	*Polytrichum hyperboreum*	10	OS-109459	0.6799	-26.28	3100 ± 20	3310 ± 50	3259 - 3289; 3333 - 3361
29	13GRØv-60	70.21573	-51.07768	856.7	Nuussuaq	*Polytrichastrum alpinum*	25	OS-106368	0.8257	-26.20	1540 ± 25	1450 ± 60	1389 - 1418, 1461 - 1484, 1489 - 1517
30	13GRØv-61	70.21562	-51.07760	859.0	Nuussuaq	*Cassiope tetragona*	0	OS-109315	0.8332	-23.50	1470 ± 30	1360 ± 30	1327 - 1383
31	13GRØv-62	70.21913	-51.07858	874.0	Nuussuaq	*Pogonatum dentatum*	0	OS-109366	0.8200	-26.00	1590 ± 25	1470 ± 60	1416 - 1463, 1480 - 1497, 1516 - 1529
32	13GRØv-64	70.21835	-51.06252	798.5	Nuussuaq	*Polytrichum hyperboreum*	0	OS-106369	0.9679	-25.24	260 ± 20	300 ± 10	289 - 308
33	13GRØv-65	70.21599	-51.05363	759.8	Nuussuaq	*Racomitrium*	120	OS-106370	0.9623	-25.81	310 ± 25	370 ± 60	308 - 326,

						canescens							360 - 366, 374 - 429
34	13GRØv-66	70.23652	-51.28443	1199.4	Nuussuaq	*Polytrichum hyperboreum*	80	OS-109367	0.5753	-25.83	4440 ± 30	5110 ± 150	4969 - 5056, 5187 - 5214, 5224 - 5235, 5244 - 5260
35	13GRØv-69	70.25624	-51.38556	1223.4	Nuussuaq	*Polytrichum piliferum*	0	OS-109460	0.6386	-25.26	3600 ± 20	3920 ± 40	3872 - 3926, 3949 - 3960
36	13GRØv-70	70.30714	-51.59230	1130.9	Nuussuaq	*Polytrichum hyperboreum*	10	OS-106453	0.6554	-25.09	3390 ± 25	3640 ± 50	3594 - 3601, 3606 - 3644, 3665 - 3685
37	13GRØv-72	70.12005	-51.15776	895.3	Nuussuaq	*Polytrichum hyperboreum*	40	OS-106371	0.7131	-26.10	2710 ± 30	2810 ± 40	2773 - 2805, 2814 - 2843
38	13GRØv-74	70.27839	-51.14834	1154.0	Nuussuaq	*Polytrichum piliferum*	0	OS-106372	0.6758	-26.37	3150 ± 25	3380 ± 20	3355 - 3399, 3435 - 3435
39	13GRØv-76	70.34024	-51.25237	1162.0	Nuussuaq	*Racomitrium lanuginosum*	0	OS-106443	0.9512	-24.60	400 ± 20	490 ± 20	471 - 503
40	13GRØv-80	70.37262	-51.40459	985.7	Nuussuaq	*Polytrichum piliferum*	5	OS-109347	0.7658	-24.32	2140 ± 25	2180 ± 110	2065 - 2083, 2106 - 2153, 2276 - 2291
41	13GRØv-82	70.36948	-51.42273	1093.1	Nuussuaq	*Polytrichum hyperboreum*	15	OS-109368	0.7310	-25.06	2520 ± 25	2620 ± 110	2516 - 2527, 2538 - 2588, 2616 - 2633, 2698 - 2729
42	13GRØv-84	70.36973	-51.44805	1214.5	Nuussuaq	*Pogonatum urnigerum and Pohlia cruda*	10	OS-106444	0.6980	-24.18	2890 ± 30	3020 ± 50	2970 - 3063
43	13GRØv-85	70.34594	-51.24895	1032.0	Nuussuaq	*Pogonatum urnigerum*	5	OS-106445	0.8179	-24.55	1610 ± 20	1480 ± 60	1421 - 1434, 1437 - 1458, 1520 - 1545
44	13GRØv-89	70.33872	-51.39925	1205.1	Nuussuaq	*Polytrichum piliferum*	800	OS-109348	0.6527	-24.58	3430 ± 30	3680 ± 40	3636 - 3718
45	13GRØv-92	70.33322	-51.36379	1192.6	Nuussuaq	*Polytrichum hyperboreum*	0	OS-106446	0.7047	-26.30	2810 ± 35	2910 ± 40	2869 - 2952
46	13GRØv-94	70.32720	-51.31510	1115.0	Nuussuaq	*Polytrichum hyperboreum*	0	OS-109349	0.8551	-26.18	1260 ± 25	1220 ± 40	1181 - 1188, 1202 - 1258
47	13GRØv-96	70.33069	-51.46105	921.3	Nuussuaq	*Polytrichum hyperboreum*	0	OS-109369	0.7794	-23.69	2000 ± 30	1950 ± 40	1904 - 1907, 1924 - 1989
48	13GRØv-99	70.32853	-51.45989	1015.3	Nuussuaq	*Polytrichum hyperboreum*	0	OS-106501	0.7981	-25.70	1810 ± 25	1760 ± 50	1709 - 1742, 1754 - 1784, 1791 - 1810
49	13GRØv-102	70.68745	-51.82557	1182.3	Uummannaq	*Pogonatum urnigerum*	0	OS-106502	0.8529	-24.77	1280 ± 20	1220 ± 40	1184 - 1207, 1234 - 1265
50	13GRØv-105	70.90286	-52.05152	1496.9	Uummannaq	*Pohlia cruda*	500	OS-106503	0.6208	-21.83	3830 ± 35	4220 ± 70	4154 - 4259, 4264 - 4287
51	13GRØv-106	70.90298	-52.05174	1493.0	Uummannaq	*Pohlia cruda*	15	OS-106520	0.5989	-23.33	4120 ± 35	4690 ± 120	4569 - 4649, 4671 - 4700, 4759 - 4807
52	13GRØv-	71.00284	-51.69842	1402.9	Uummannaq	*Polytrichastrum*	90	OS-106522	0.5978	-25.44	4130 ± 30	4690 ± 110	4579 - 4651,

	107					*alpinum*							4670 - 4702, 4758 - 4770, 4780 - 4808
53	13GRØv-108	71.00279	-51.69784	1401.2	Uummannaq	*Pohlia cruda*	200	OS-109461	0.6200	-22.23	3840 ± 20	4220 ± 60	4160 - 4170, 4178 - 4200, 4227 - 4260, 4262 - 4288
54	13GRØv-110	70.97365	-51.42092	1206.1	Uummannaq	*Polytrichum hyperboreum*	50	OS-106504	0.8232	-23.70	1560 ± 25	1460 ± 60	1409 - 1421, 1433 - 1438, 1457 - 1520

Supplemental References

Anderson, R. K., Miller, G.H., Briner, J.P., Lifton, N.A., and DeVogel, S.B., 2008, A millennial perspective on Arctic warming from 14C in quartz and plants emerging from beneath ice caps: Geophysical Research Letters, v. 35, L01502.

Bakke, J., Lie, Ø., Nesje, A., Dahl, S.O., Paasche, and Ø., 2005, Utilizing physical sediment variability in glacier-fed lakes for continuous glacier reconstructions during the Holocene, northern Folgefonna, western Norway: The Holocene, v. 15, p. 161-176.

Balascio, N.L., D'Andrea, W.J., and Bradley, R.S., 2015, Glacier response to North Atlantic climate variability during the Holocene: Climate of the Past, v. 11, p. 2009-2036.

Balco, G., Stone, J.O., Lifton, N.A. and Dunai, T.J., 2008, A complete and easily accessible means of calculating surface exposure ages or erosion rates from 10 Be and 26 Al measurements: Quaternary Geochronology, v. 3, p.174-195.

Blaauw, M., 2010, Methods and code for 'classical'age-modelling of radiocarbon sequences: Quaternary Geochronology, v. 5, p. 512-518.

Briner, J.P., Stewart, H.A.M., Young, N.E., Philipps, W. and Losee, S., 2010, Using proglacial threshold lakes to constrain fluctuations of the Jakobshavn Isbræ ice margin, western Greenland, during the Holocene: Quaternary Science Reviews, v. 29, p.3861-3874.

Briner, J.P., et al., 2016, Holocene climate change in Arctic Canada and Greenland: Quaternary Science Reviews, (*in press*).

Croudace, I.W., Rindby, A., and Rothwell, R.G., 2006, ITRAX: description and evaluation of a new multi-function X-ray core scanner. In: Rothwell, R.G. (Ed.), New Techniques in Sediment Core Analysis: Special Publications, 267, Geological Society, London, p. 193–207.

Dahl, S. O., Bakke, J., Lie, Ø., and Nesje, A., 2003, Reconstruction of former glacier equilibrium line altitudes based on proglacial sites: an evaluation of approaches and selection of sites: Quaternary Science Reviews, v. 22, p. 275–287.

Falconer, G., 1966, Preservation of vegetation and patterned ground under a thin ice body in northern Baffin Island, NWT: Geogr. Bull, v. 8, p. 194-200.

Geirsdottir, A., Miller, G.H., Larsen, D.J., and Olafsdottir, S., 2013, Abrupt Holocene climate transitions in the northern North Atlantic region recorded by synchronized lacustrine records in Iceland: Quaternary Science Reviews, v. 70, p. 48-62.

Ives, J., 1962, Indications of recent extensive glacierization in north-central Baffin Island, NWT: Journal of Glaciology, v. 4, p. 197-205.

Jansson, P., Rosqvist, G., and Schneider, T., 2005, Glacier fluctuations, suspended sediment flux and glacio-lacustrine sediments: Geografiska Annaler ,v. 87, p. 37–50.

Koerner, R.M., 2005, Mass balance of glaciers in the Queen Elizabeth Islands, Nunavut, Canada: Annals of Glaciology, v. 42, p. 417–423, doi:10.3189/172756405781813122.

Kohl, C.P. and Nishiizumi, K., 1992, Chemical isolation of quartz for measurement of in-situ produced cosmogenic nuclides: Geochimica et Cosmochimica Acta, v. 56, p.3583-3587.

LaFarge, C., Williams, K.H., and England, J.H., 2013, Regeneration of Little Ice Age bryophytes emerging from a polar glacier with implications of totipotency in extreme environments: PNAS, v. 110, p. 9839–9844.

Lal D., 1991, Cosmic ray labeling of erosion surfaces: in situ nuclide production rates and erosion models: Earth and Planetary Sciences Letters, v. 104, p. 424–439.

Margreth, A., Dyke, A.S., Gosse, J.C., and Telka, A.M., 2014, Neoglacial ice expansion and late Holocene cold-based ice cap dynamics on Cumberland Peninsula, Baffin Island, Arctic Canada: Quaternary Science Reviews, v. 91, p. 242-256.

Miller, G.H., Briner, J.P., Refsnider, K.A., Lehman, S.J., Geirsdóttir, Á., Larsen, D.J. and Southon, J.R., 2013a, Substantial agreement on the timing and magnitude of Late Holocene ice cap expansion between East Greenland and the Eastern Canadian Arctic: A commentary on Lowell et al., 2013: Quaternary Science Reviews, v.77, p. 239-245.

Miller, G.H., Lehman, S.J., Refsnider, K.A., Southon, J.R., and Zhong, Y., 2013b, Unprecedented recent summer warmth in Arctic Canada: Geophysical Research Letters, v. 40, p. 1-7.

Miller , G.H., Landvik, J., and Lehman, S.J., *in press*, Episodic Neoglacial snowline descent and glacier expansion on Svalbard reconstructed from the 14C ages of ice-entombed plants: Quaternary Science Reviews.

Nesje, A., 1992, A piston corer for lacustrine and marine sediments: Arctic and Alpine Research, p. 257-259.

Nesje, A., Dahl, S. O., Andersson, C., and Matthews, J. A., 2000, The lacustrine sedimentary sequence in Sygneskardvatnet, western Norway: a continuous, high-resolution record of the Jostedalsbreen ice cap during the Holocene: Quaternary Science Reviews, v.19, p. 1047–1065.

Nishiizumi, K., Imamura, M., Caffee, M.W., Southon, J.R., Finkel, R.C. and McAninch, J., 2007, Absolute calibration of 10 Be AMS standards: Nuclear Instruments and Methods in Physics Research Section B: Beam Interactions with Materials and Atoms, v. 258, p. 403-413.

Nishiizumi, K., Winterer, E.L., Kohl, C.P., Klein, J., Middleton, R., Lal, D. and Arnold, J.R., 1989, Cosmic ray production rates of 10Be and 26Al in quartz from glacially polished rocks: Journal of Geophysical Research: Solid Earth, v. 94, p.17907-17915.

Noh, M.J., and Howat, I.M., 2015, Automated stereo-photogrammetric DEM generation at high latitudes: Surface Extraction from TIN-Based Search Minimization (SETSM) validation and demonstration over glaciated regions: GIScience and Remote Sensing, doi:10.1080/15481603.2015.1008621.

Reimer, P.J., et al., 2013, IntCal13 and Marine13 radiocarbon age calibration curves 0–50,000 years cal BP: Radiocarbon, v. 55, p.1869-1887.

Røthe, T.O., Bakke, J., Vasskog, K., Gjerde, M., D'Andrea, W.J., and Bradley, R.S., 2015, Arctic Holocene glacier fluctuations reconstructed from lake sediments at Mitrahalvøya, Spitsbergen: Quaternary Science Reviews, v. 109, p. 111–125, doi:10.1016/j.quascirev.2014.11.017.

Rothwell, R.G., Hoogakker, B., Thomson, J., Croudace, I.W., and Frenz, M., 2006, Turbidite emplacement on the southern Balearic Abyssal Plain (western Mediterranean Sea) during Marine Isotope Stages 1–3: an application of ITRAX XRF scanning of sediment cores to lithostratigraphic analysis. In: Rothwell, R.G. (Ed.), New Techniques in Sediment Core Analysis. Special Publications, 267. Geological Society, London, p. 65–78.

Smith, J.G., 2003, Aspects of the loss-on-ignition (LOI) technique in the context of clay-rich, glaciolacustrine sediments: Geografiska Annaler: Series A, Physical Geography, v. 85, p. 91-97.

Stone J.O., 2000, Air pressure and cosmogenic isotope production: Journal of Geophysical Research, v. 105, p. 23,753–23,759.

van de Berg, W.J., van den Broeke, M., Ettema, J., van Meijgaard, E., and Kaspar, F., 2011, Significant contribution of insolation to Eemian melting of the Greenland Ice Sheet: Nature Geoscience, v. 4, p. 679–683, doi:10.1038/ngeo1245.

Vasskog, K., Paasche, Ø., Nesje, A., Boyle, J.F., and Birks, H.J.B., 2012, A new approach for reconstructing glacier variability based on lake sediments recording input from more than one glacier: Quaternary Research, v. 77, p.192-204.

Young, N.E., Schaefer, J.M., Briner, J.P., Goehring, B.M., 2013, A ^{10}Be production-rate calibration for the Arctic: Journal of Quaternary Science, v. 28, p. 515-526.

Young, N.E., Schweinsberg, A.D., Briner, J.P., Schaefer, J.M., 2015, Glacier maxima in Baffin Bay during the Medieval Warm Period coeval with Norse settlement: Science Advances, v. 1, e1500806.